Cirrus and mid level clouds remote sensing programme

P. H. Flamant, H. Chepfer, L. Sauvage, J. Pelon
Institut Pierre Simon Laplace (IPSL), France

Cirrus clouds and mid-level clouds are important modulators of the earth's radiative balance. Climate models suggest that cirrus may produce a positive or a negative feedback response to global warming depending on cloud optical depth, altitude, particle shapes, and size distributions. A parametrization of the cirrus radiative characteristics is challenging for these clouds are composed largely of ice crystals exhibiting a wide range of shapes, sizes and orientations and inhomogeneous. In addition, mid-level clouds and less often cirrus are composed of a mixture of ice crystals with supercooled liquid water. In order to simulate the radiative properties of cirrus and mid level clouds in GCM and mesoscale models, accurate measurements of their microphysical and structural characteristics are needed. These characteristics can be documented during i ntense field observation experiments or routine measurements. Ultimately, a monitoring of cirrus and mid-level cloud at large scale by satellite is necessary. At the present, satellite-borne radiometers do provide with global coverage, but suffer a lack of accuracy in height assignment and retrieved radiative properties.

A "Cirrus and mid level clouds remote sensing programme" in conducted at LMD for climate and meteorological applications. Several activities are conducted in the framework of this programme : i) process studies involving interaction between radiation and dynamics, ii) parametrization of optical and sctuctural characteristics, iii) validation of POLDER/ ADEOS. The LMD data set is made of various contributions : i) ground based lidar and radiometric measurements since January 1993 carried out at Palaiseau, ii) airborne lidar (LEANDRE) measurements during international field campaigns i.e. E-LITE, EUCREX'94, ECRIN'96, iii) POLDER/ADEOS validation. Regarding the determination of actual optical depth and crystals size in cirrus clouds, we recently conducted an experiment with a multi-field of view lidar receiver. For the POLDER/ADEOS validation, several ground based lidars are currently involved : two CARS site in Oklahoma and Manus, contribution made by J. Spinhirne, Buenos Aires, contribution made by M. Lavorato, Tsukuba, contribution made by A. Asano.The "Cirrus and mid-level clouds remote sensing programme" will be presented during the workshop.

Objectives

- **Climatology of high- and mid-cloud properties at mid latitudes**
  - Routine measurements (time series), fields campaigns (spatial coverage),
  - Sets of relevant parameters
  - Correlations among parameters
- **Parametrization**
- **Case studies**
  - **Radiative impact at mesoscale**
    - Radiative transfer model, Microphysics
  - **Cloud-aerosols interaction**
  - **Mesoscale meteorology**
    - Radiation/Microphysics/Dynamics interaction
    - Life cycle, Seeding processes
- **Remote sensors synergism**
  - Instruments grouping, Improvement of inversion techniques
  - Platforms configuration

MDS lidar workshop Hakone, Japan, 11-13 March, 1998

Synergetic studies

- **Airborne payload and Ground based instrument grouping**
  - **EUCREX in 1994, in Brittany, France**
    - Backscatter lidar 0.53 μm, 1.06 μm, Δ
    - POLDER
    - IR-narrow beam radiometer
  - **ECRIN in 1996, in Brittany, France**
    - Backscatter lidar 0.53 μm, 1.06 μm, Δ
    - Mid IR-Spectrometer (SICAP)
    - Infrared imager (CIRAP)
    - IR-narrow beam radiometer
  - **RALI (Radar-lidar) in 1999**
    - *TRAC and CARL in 1998*
- **Spaceborne payload**

Pierre H. Flamant Institut Pierre Simon Laplace

EUCREX'94.


AVHRR

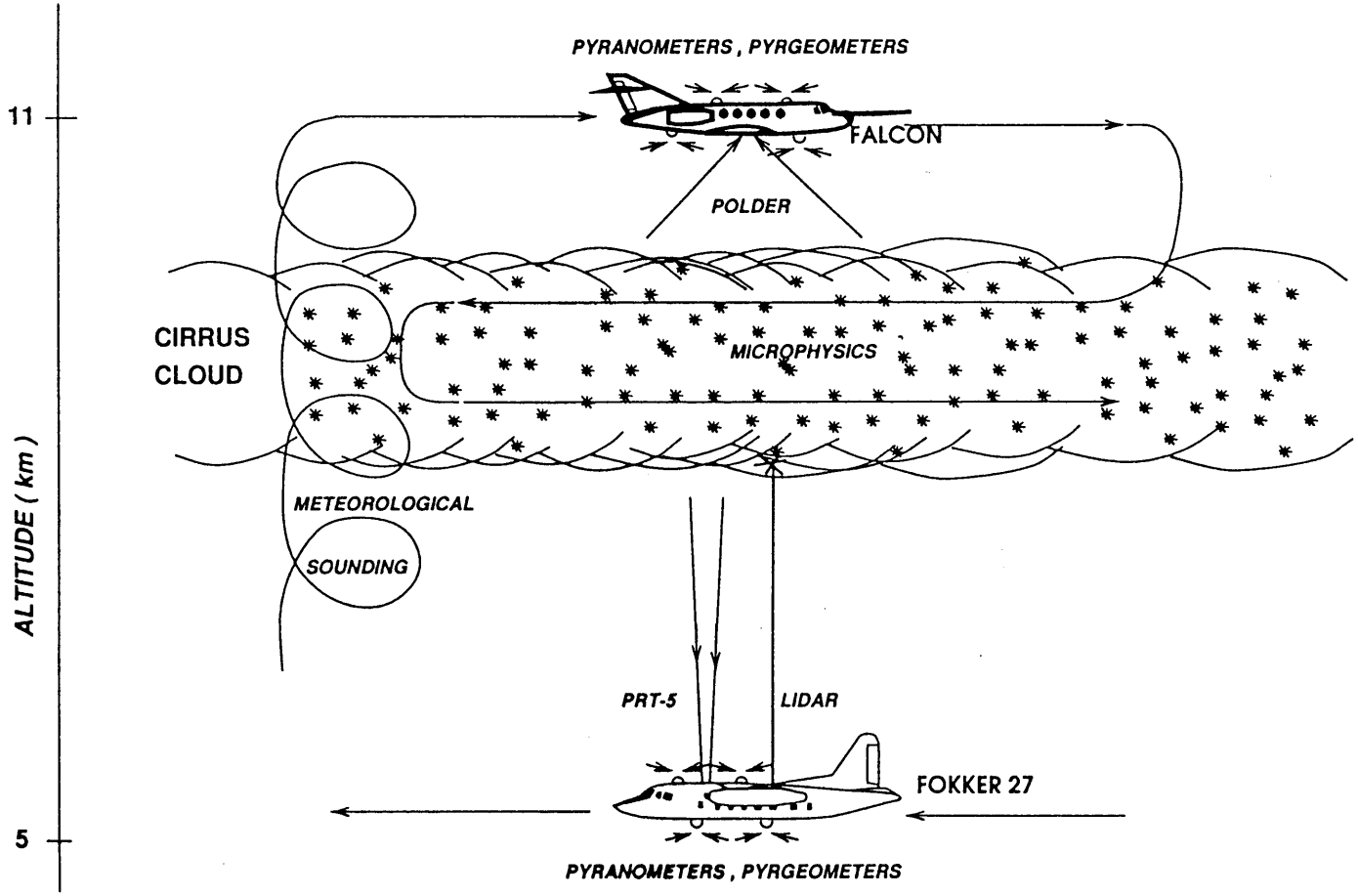
PYRANOMETERS , PYRGEOMETERS
11
FALCON
POLDER
CIRRUS
CLOUD
MICROPHYSICS
METEOROLOGICAL
SOUNDING
ALTITUDE (km)
PRT-5
LIDAR
FOKKER 27
5
PYRANOMETERS , PYRGEOMETERS

AVHRR (ch 4) - 17th of April 1994

8h55

16h20

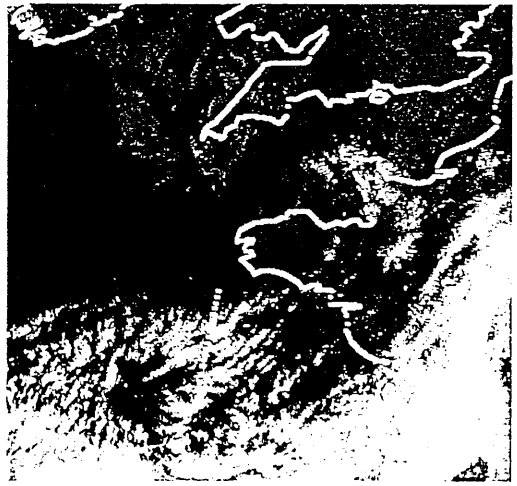

Comparisons models / measurements

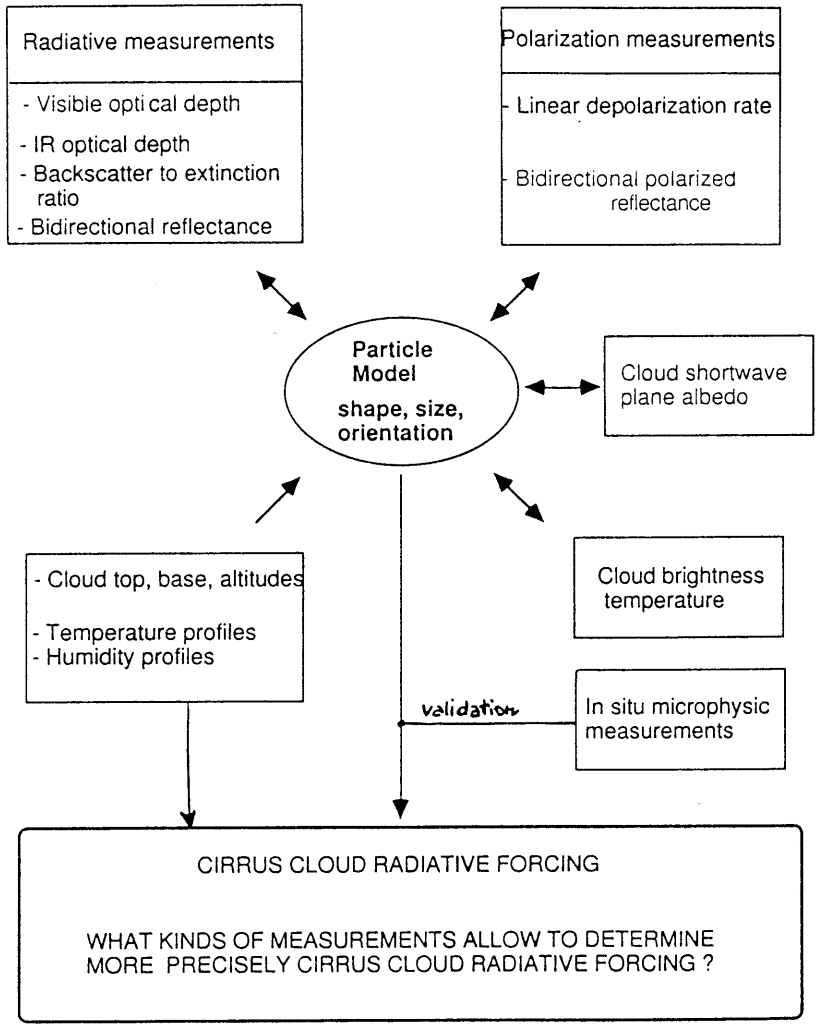

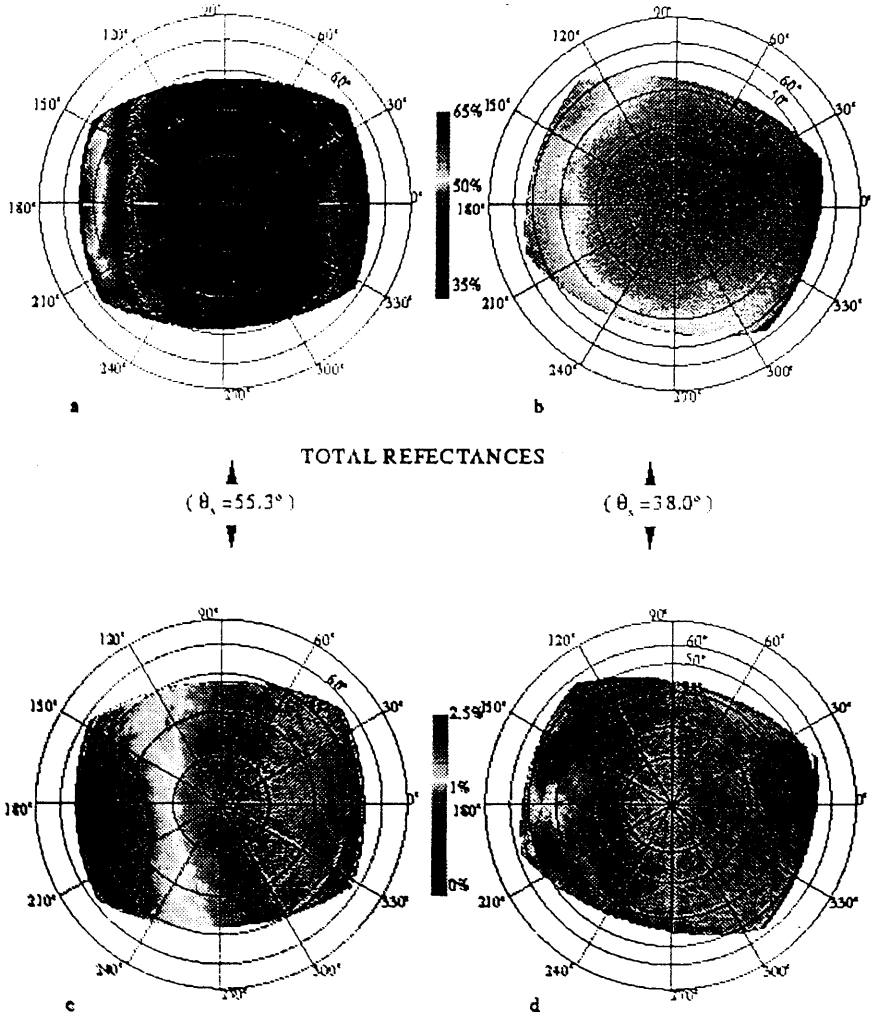

POLARIZATION AND DIRECTIONALITY OF THE EARTH REFLECTANCES

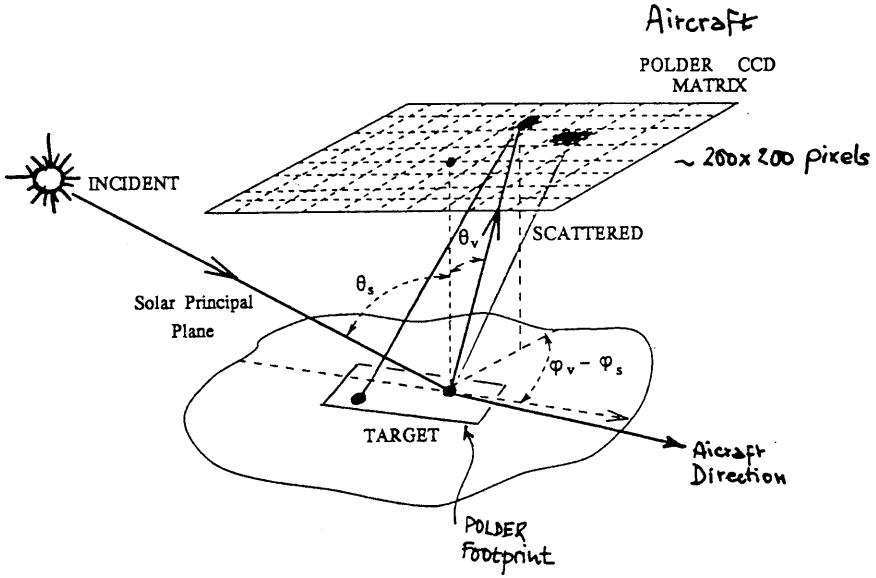

Channel = 443 nm *
670 nm
763 nm
765 nm
865 nm *

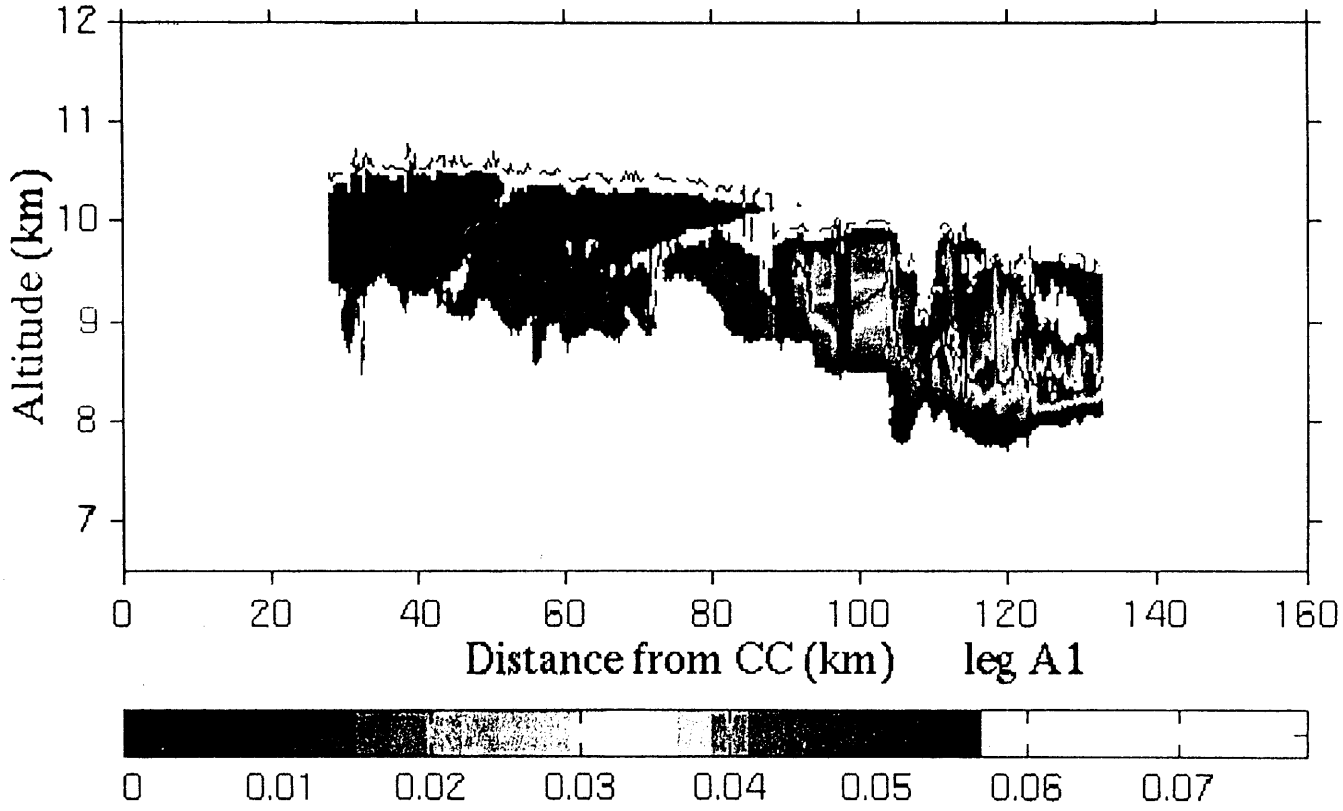
12
11
10
9
8
7
Altitude (km)
0
20
40
60
80
100
120
140
160
Distance from CC (km) leg A1
0
0.01
0.02
0.03
0.04
0.05
0.06
0.07

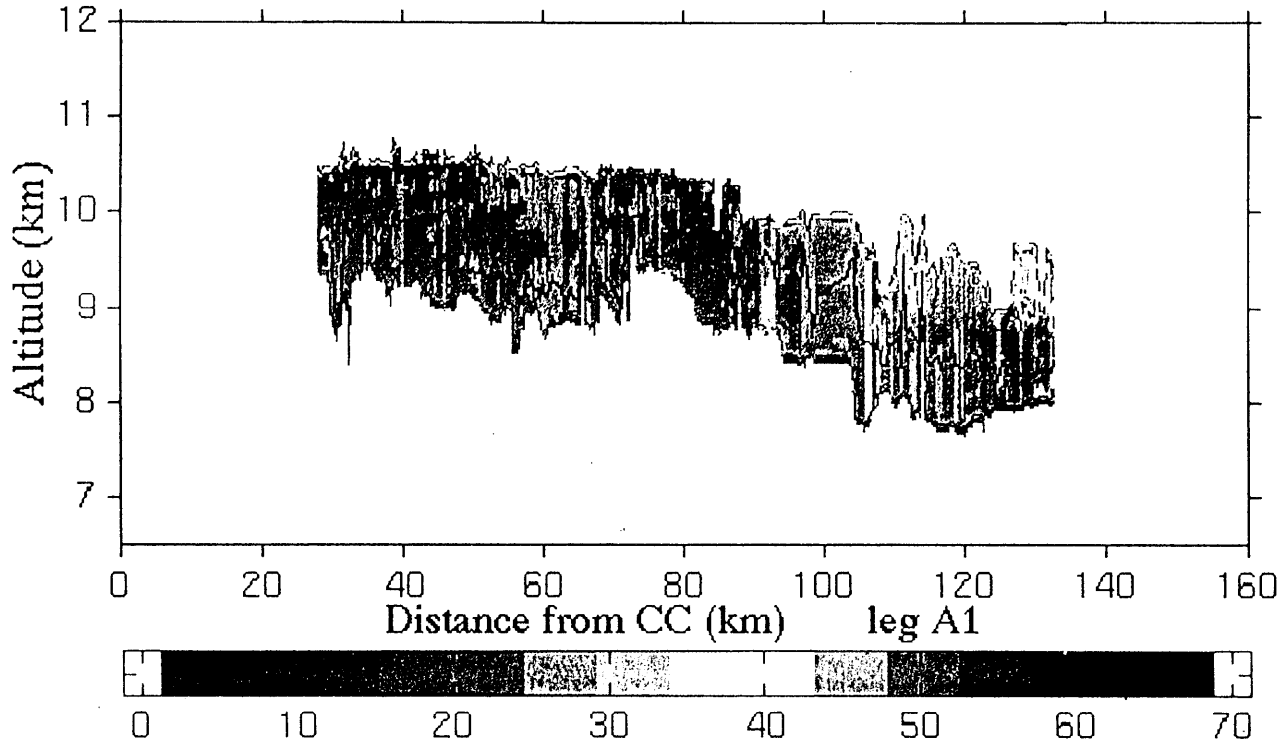
12
11
10
9
8
7
Altitude (km)
0
20
40
60
80
100
120
140
160
Distance from CC (km) leg A1
0
10
20
30
40
50
60
70

Cirrus cloud radiative forcing: 17th of April 1994

* Estimation based on microphysical models determined previously

-> Short-wave radiative forcing

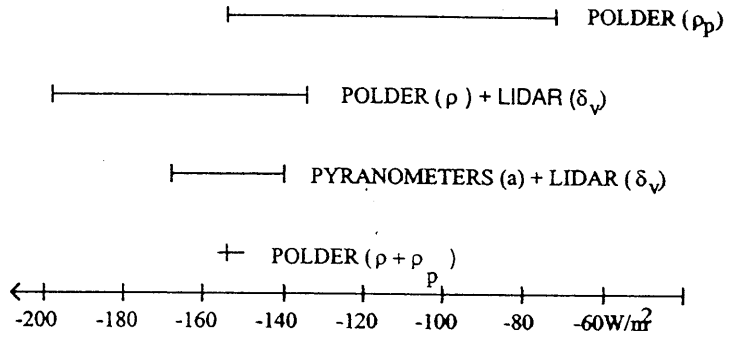

-> Long-wave radiative forcing

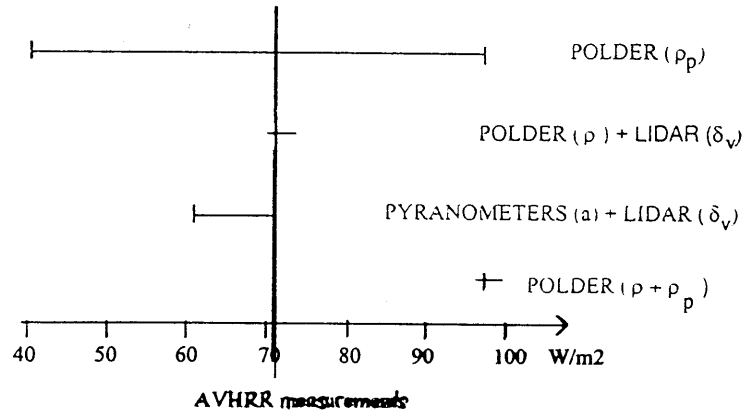

POLDER/ADEOS : Validation for Cirrus clouds

Contributions from : P. Goloub (LOA), J. Spinhirne (NASA/GSFC), M. Lavorato (Argentina), S. Asano (MRI, Japan)

○ **Comparison of cloud properties derived from POLDER vs. GB lidar/radiometer**

○ Parameters	Height, optical depth, Ice/Liquid water discrimination Ice Water Content (IWC), r_e effective radius	
○ Direct comparison :	Water phase	Δ by lidar, Rainbow by POLDER
	Height	β(z) by lidar, Atmospheric pressure by POLDER
	Detection threshold	Optical depth
○ Level 2 products	Optical depth and Microphysics in inversion code	

POLDER PRODUCTS

Cloud parameter	Inversion method	Measured quantity
Altitude	- Rayleigh pressure method (Goloub et al 1994)	Bidirectional polarized reflectances at 443 nm and 864 nm
	- Differential absorption method - O2 pressure (Fisher et al 1991, Parol et al 1994)	Bidirectional reflectances at 765 nm (wide and narrow chanels)
Water phase (ice/liquid)	- Absence or presence of rainbow θ=140° (Goloub et al 1994)	Bidirectional polarized reflectances at 864nm around θ=140°.
	- Liquid/ice signature for scattering angles lower than 110°	*Bidirectional polarized reflectances at 864nmfor scattering angles lower than 110°*
Optical depth	Inversion using an a priori microphysical model (r_e=10 µm)	Bidirectional reflectances at 443, 670, 864 nm

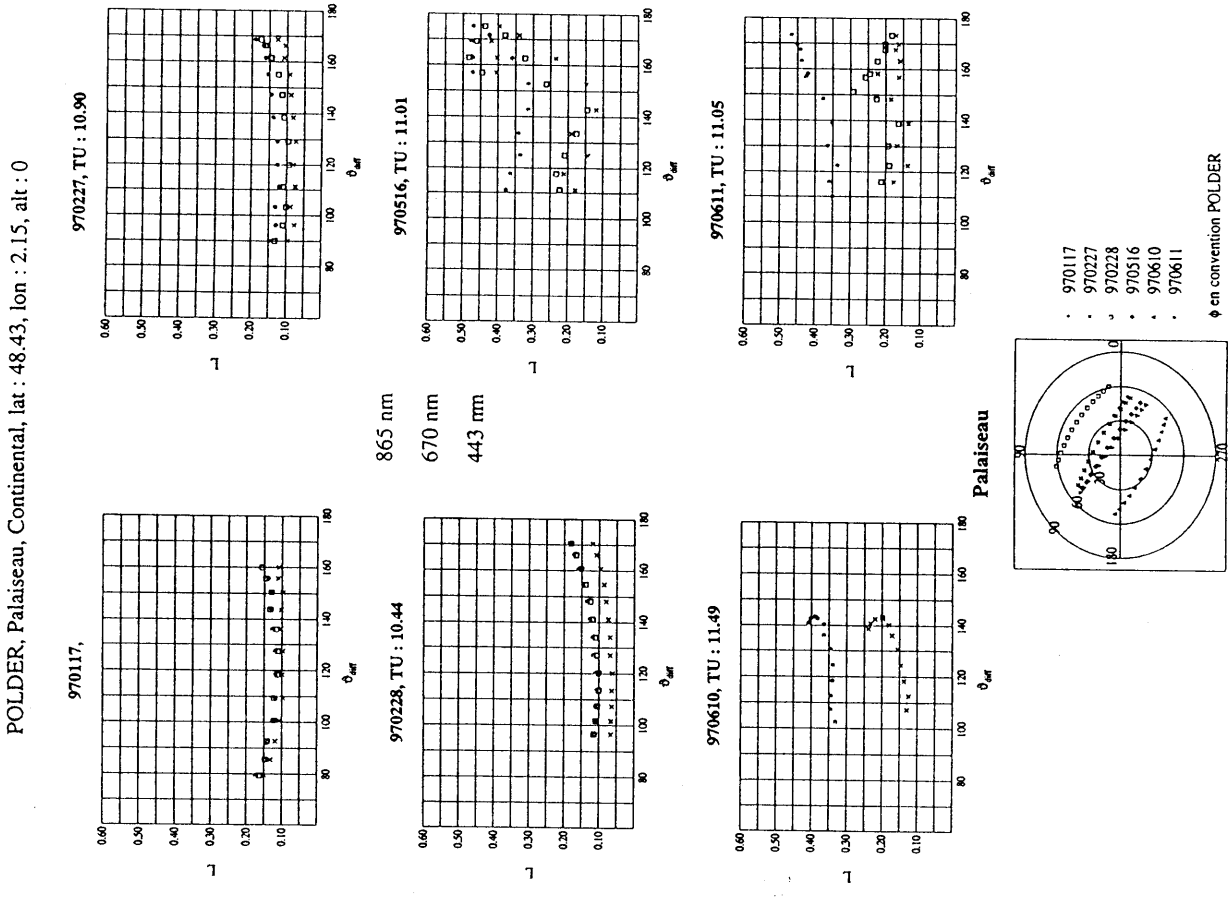

Lidar Measurements

Cases of cirrus clouds observations performed simultaneously with ground-based lidars and POLDER/ADEOS overpasses

- **Palaiseau** (48.43° N, 2.15° E): **11:00 TU**
  17/01 - 27/02 - 28/02 - 16/05 - 04/06 - 10/06 - 11/06

- **Oklahoma ARM** (36.06° N, 97.49° W): **17:50 TU**
  09/11 - 10/11 - 05/12 - 06/12 - 09/12 - 10/12 - 21/12 - 22/12 - 28/12
  January to June -> selection to be done

- **Manus** (2.06° S, 147.44° W): **20:30 TU**
  Weeks of 16-22 March and 23-29 March
  Weeks of 13-19 April and 20-26 April

- **Buenos Aire** (34.36° S, 57.6° W): **15:00 TU**
  11/11 - 18/11 - 11/12 - 20/01 - 15/04 - 28/04 - 16/05 - 19/05

- **Japan** (36°N, 140.1°E): **01:50 TU**
  11/05 - 13/05 - 29/05 - 30/05 - 03/06 - 13/06 - 25/06

Hélène Chepfer Institut Pierre Simon Laplace

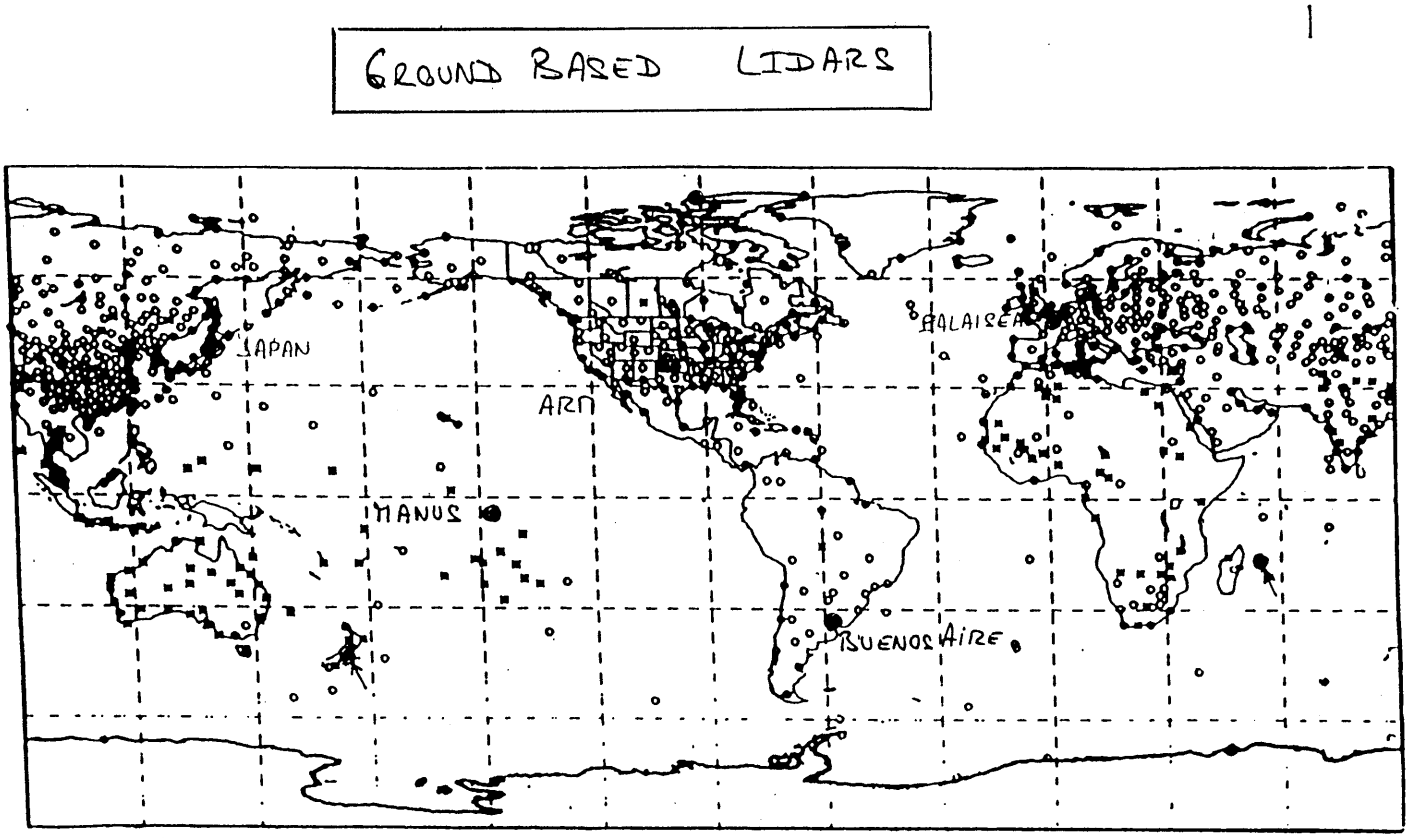

Fig. 2. A typical set of upper-air soundings at 1200 UTC (Dey 1989).

0612

Lidar => 2 couches.

Poldar => 2 méthodes donne valeur intermédiaire
la même chose (z = 8.5 km)
... hasard ?

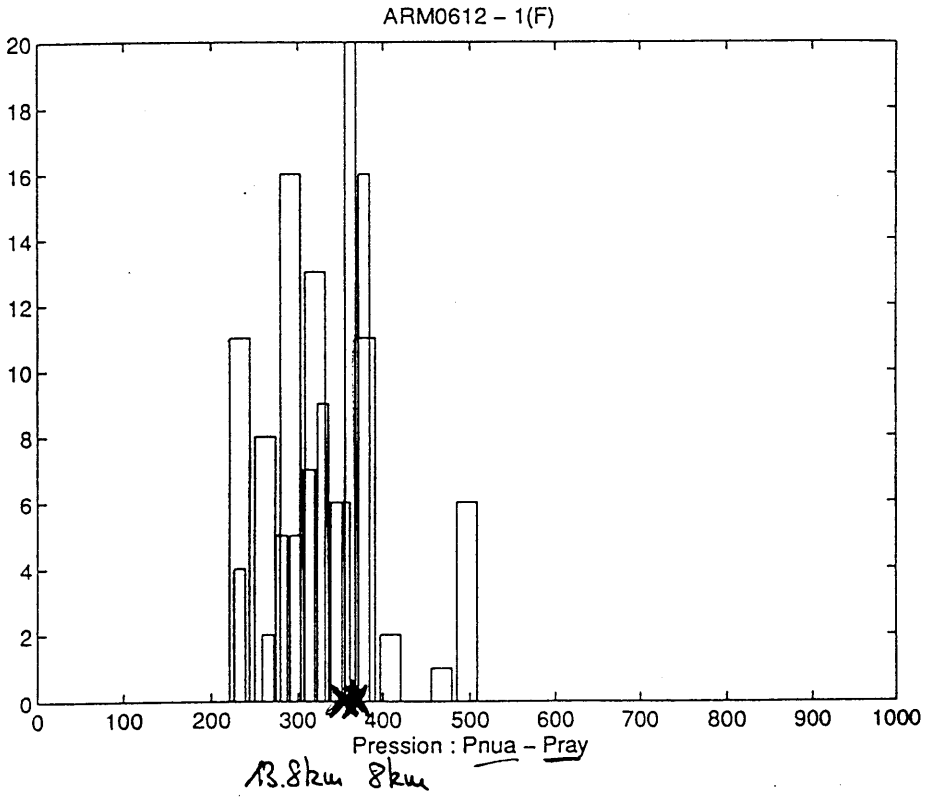

13.8km 8km

Pantal : Pnua = 374.8 → 8.5 km
Pray = 372.3 → 8.5 km

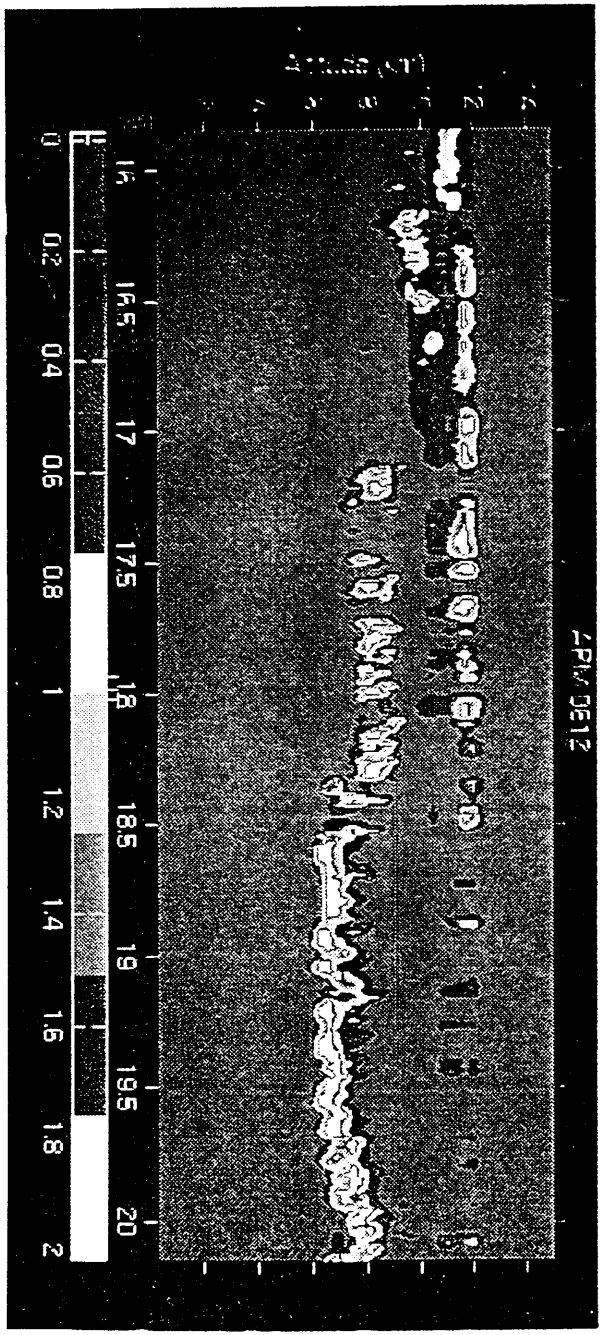

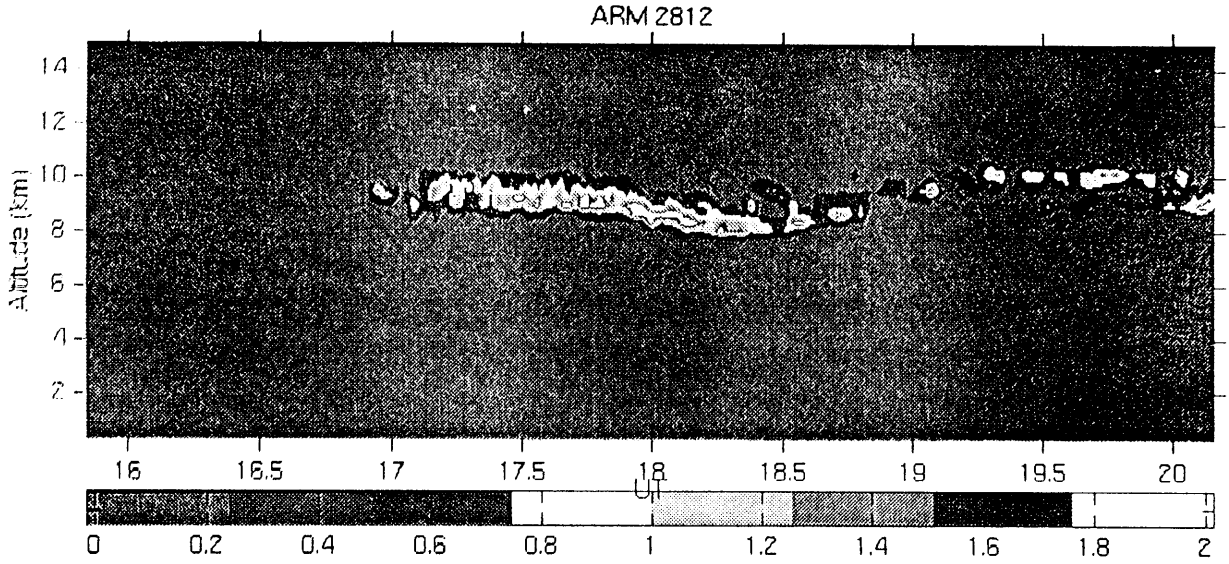

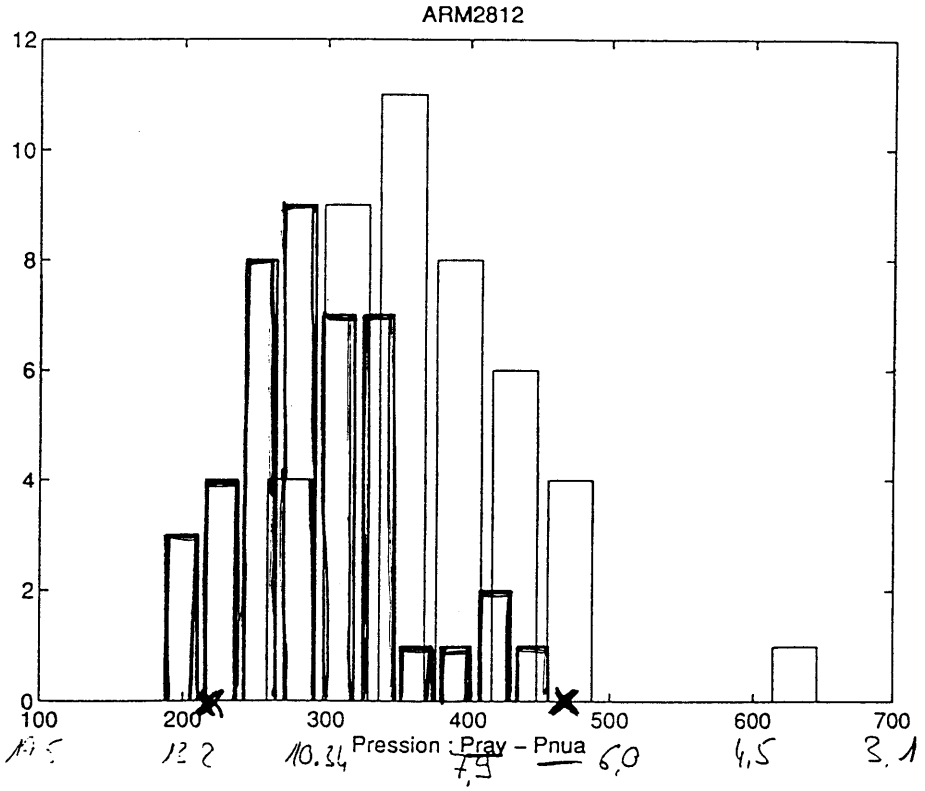

Pixel central $P_{ray} = 477.3 \rightarrow z = 6.4$ km

$P_{nua} = 206.8 \rightarrow 13.5$ km

"MFOV" Backscatter Lidar
Semi transparent Clouds

- **Principle** — Multiple scattering in semi-transparent clouds depends on particle size
- **Objective** — True optical depth, mean effective radius and IWC
- **Lidar Ambiguity** — backscatter-to-extinction lidar ratio (k)
  Multiple scattering factor (η)
  Forward scattering at 0° or balistic contribution (R)
  Scattering phase function around π ($p(\pi \pm \varepsilon)$)

- **Direct Problem** *(Nicolas et al 1997)*
  - Single scattering approximation
    Multiple forward scatterings (diffractions) but one single scattering event $\eta \cong 0.50 - R$
    Two characterisric angles : $\theta_c = \frac{L\,\theta_R}{(z-L)}$ and $\theta_d = \frac{\lambda}{2\,r_{eq}}$
    Multiple scattering : $\frac{\theta_c}{\theta_d} \approx 1$
    Single backscatter event : $\delta \leq [2(1-g)]^{-1}$
  - Backpropagated receiver *(Nicolas 1997, Katsev et al 1997)*
  - Molecular scattering beyond the cloud (mean value for r_e)
- **Inverse problem :**
  - Semi analytical solution
  - Variational method
- **Preliminary experimental results**
  - 5 FOV : 0.5 mrad to 5 mrad

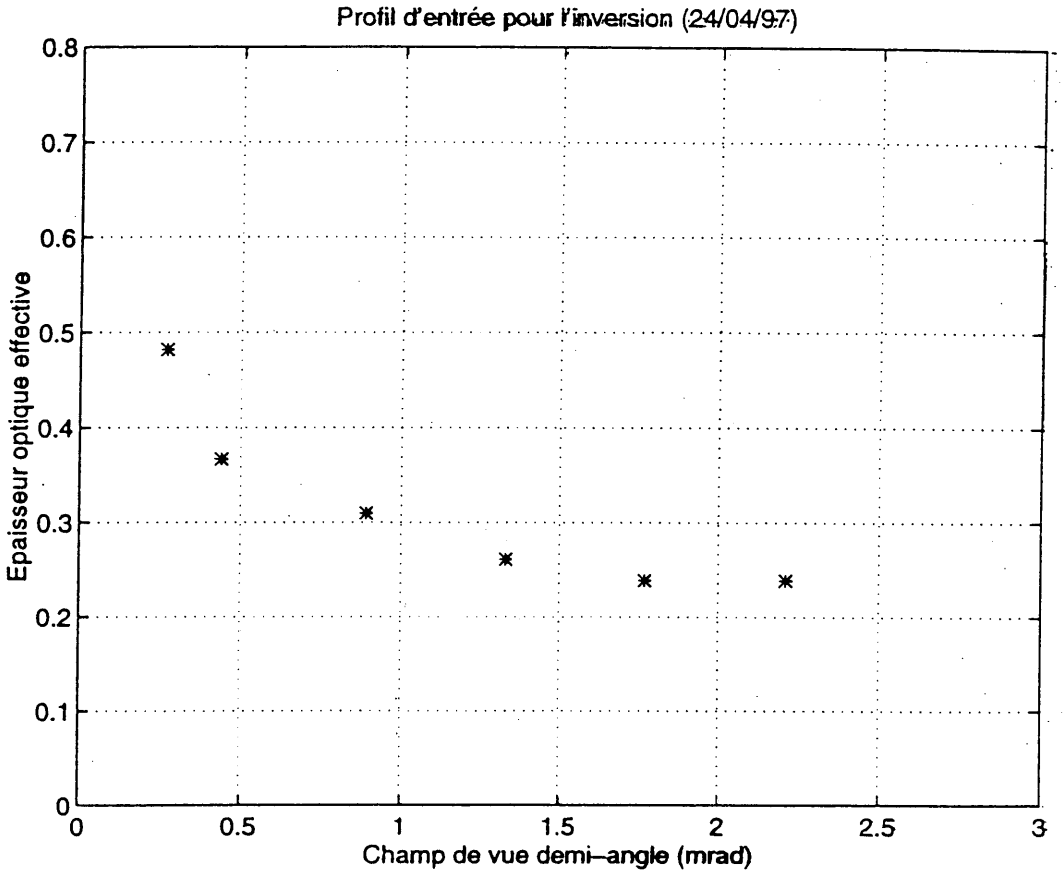
Profil d'entrée pour l'inversion (24/04/97)
Epaisseur optique effective
Champ de vue demi-angle (mrad)
0.8
0.7
0.6
0.5
0.4
0.3
0.2
0.1
0
0
0.5
1
1.5
2
2.5
3

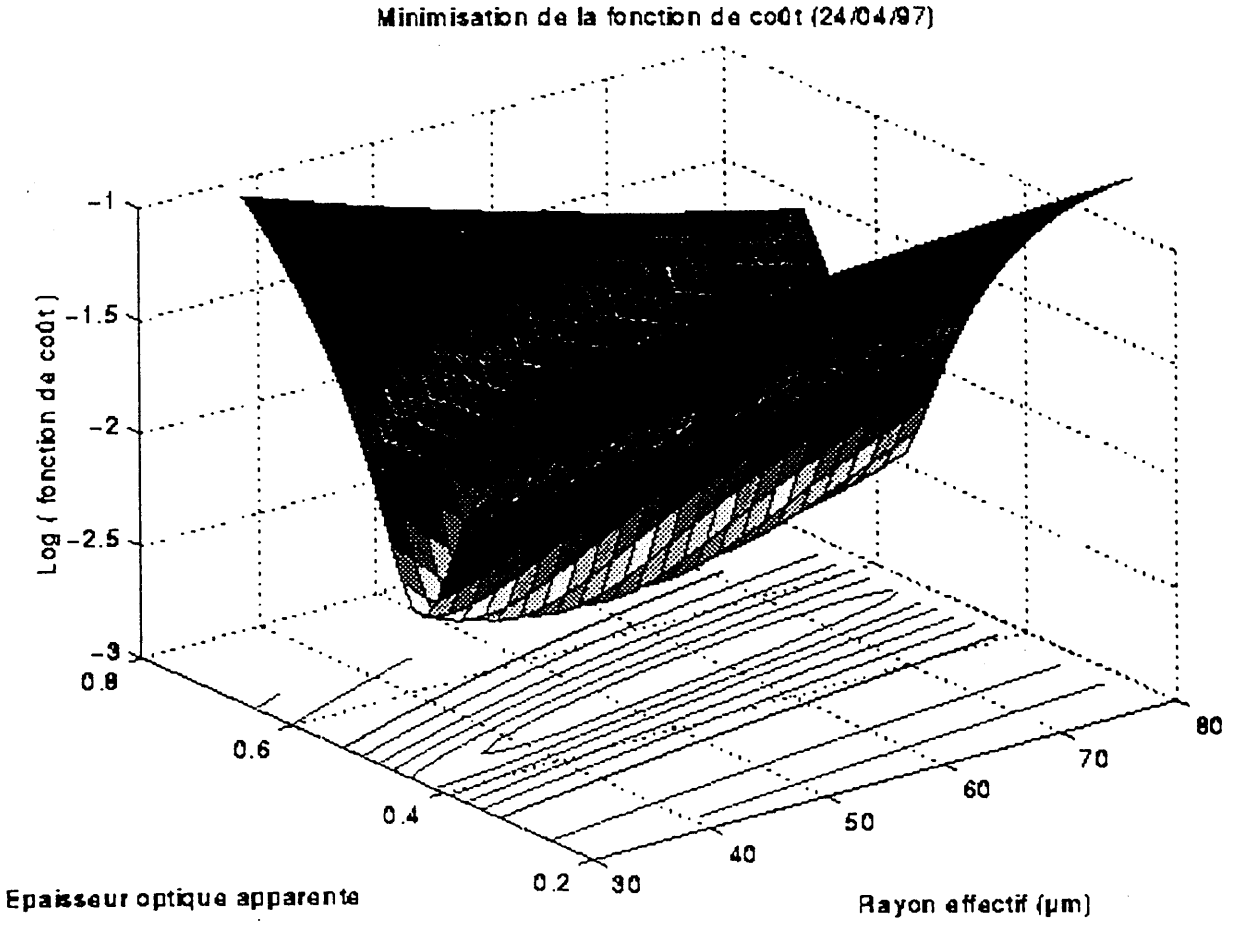
Minimisation de la fonction de coût (24/04/97)
Log (fonction de coût)
-1
-1.5
-2
-2.5
-3
0.8
0.6
0.4
0.2
Epaisseur optique apparente
30
40
50
60
70
80
Rayon effectif (µm)

Ground-based Instrumented Site at École Polytechnique
Institut Pierre Simon Laplace

Lidars :

LMD	Transportable Wind Lidar (10,6 µm) with 3D-sampling capability
ONERA/ IPSL	Transportable Wind Lidar (2 µm)
SA	LEANDRE-2 DIAL/Water vapor (0.73 µm)
LMD	Backscatter lidar (0,53 µm /1,06 µm/Δ) upward looking (10° from zenith)

Radars :

CETP	"Ronsard" (5,5 GHz), mobile (2 vans)
CETP	94 GHz-Radar (RALI)

Supplementary instruments :

LMD/LSCE	Visible and IR radiometers
LMD	In situ measurements
Météo-France	2 soundings per day (at 00:00 et 12:00 TU) at nearby station (12 km)
LSCE	Instrumented mast

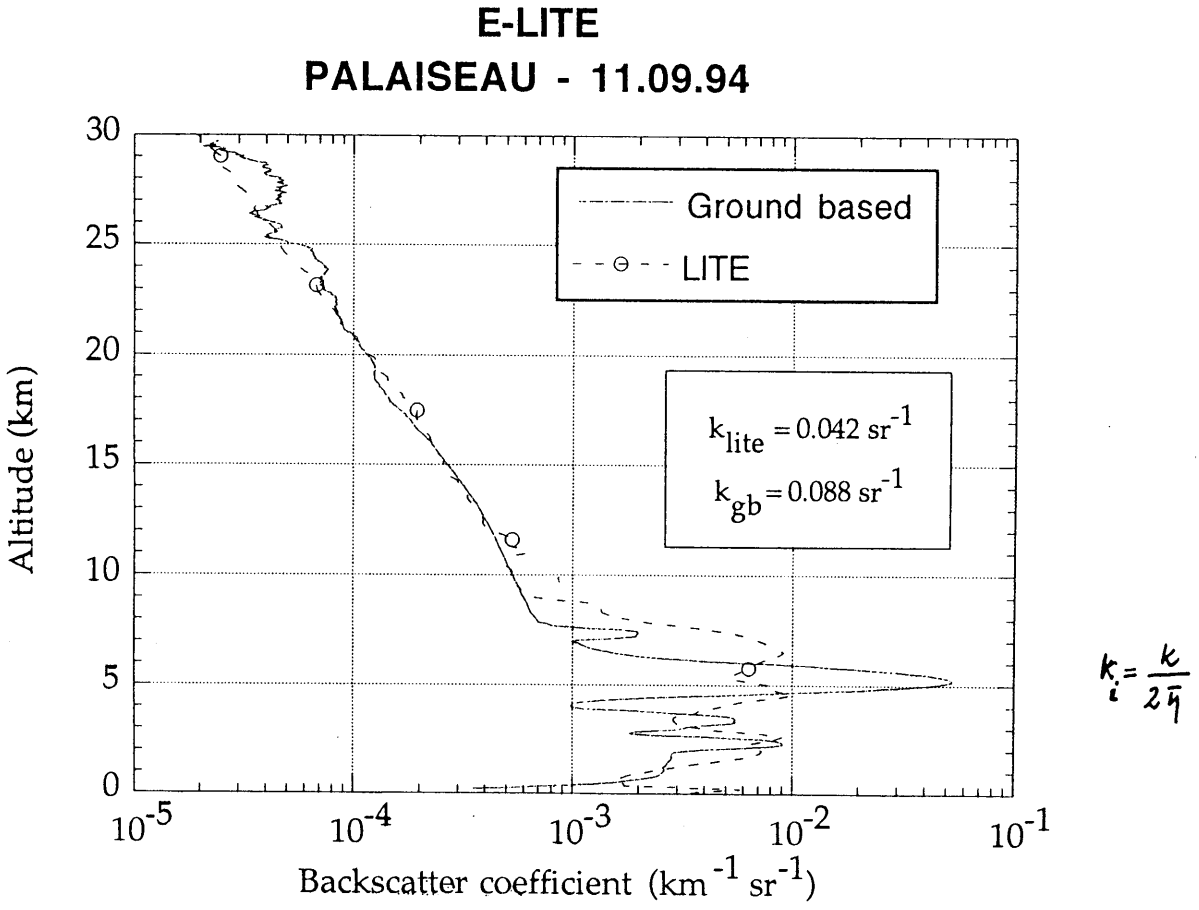

$k_i = \frac{k}{2\bar{\eta}}$

données avions.

Les figures 3.12 représentent la transmission atmosphérique en fonction du coefficient de rétrodiffusion intégré sur tout le nuage pour LITE, ALEX et LEANDRE. Comme on a dû moyenner sur 100 tirs les fichiers LITE pour réduire notablement le bruit, nous disposons de peu de points de mesures. Cependant, en tenant compte du fait que le carré de la transmission $T_a^2 = \exp(-2\tau_a)$ varie linéairement avec β_{int} (cf équation 3.1), et que, quand la transmission est nulle, β_{int} vaut $k_a/2$, on arrive à regrouper certains points pour déterminer une valeur de la fonction de phase apparente. Les regroupements de mesures sont plus faciles à observer sur les mesures ALEX.

Les valeurs de k_a restituées sur les différentes orbites et pour les différents instruments ont été reportées dans le tableau 3.5. On remarque alors que, pour un même type d'observation, c'est à dire pour une même orbite d'étude, la fonction de phase apparente de LITE est supérieure à celles obtenues par les avions, qui, elles sont relativement proches l'une de l'autre. Le rapport peut atteindre des valeurs proches de 2. La figure 3.13 montre l'évolution de la fonction de phase apparente obtenue

N° d'orbite	32		33	46	47	78		79	80	128
k_a (sr^{-1}) LITE	0,062	0.090	0,038		0,039	0,039	0.051	0,025 0,039	0,052	
k_a (sr^{-1}) FALCON	0,044	0,065	0,023			0,028				0,028
k_a (sr^{-1}) ARAT			0,022	0,046		0,029	0,033			0,029
k_a(FALCON)/ k_a(ARAT)			1,04			0,85	0,96			
k_a(LITE)/ k_a(Avions)	1,38	1,44	1,65-1,72			1,18	1,82		1,79	

TAB. 3.5 – *Valeurs de la fonction de phase apparente k_a pour les différentes types de mesures et pour différentes orbites.*

à partir des mesures avion en fonction de la température moyenne du nuage. Les mesures avions de la campagne E-LITE sont proches de celle obtenues par Platt et

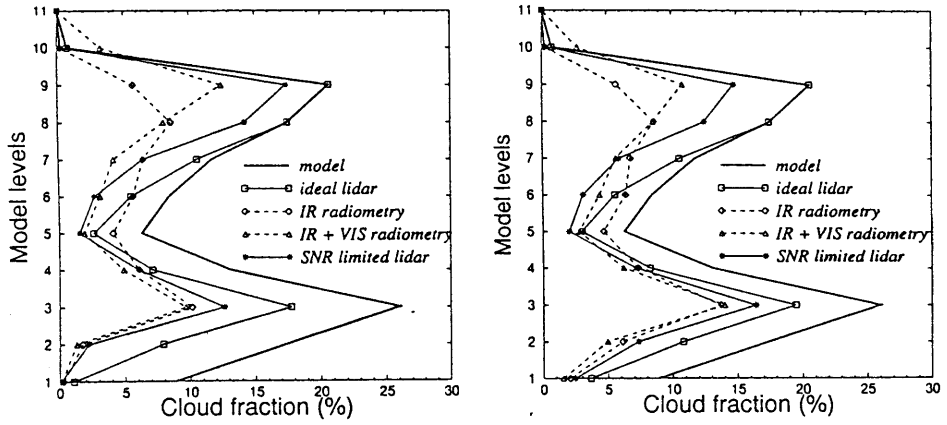

(a) Maximum Cloud overlap assumption

(b) Random cloud overlap assumption

Figure 5. Comparison of lidar- and radiometer-retrieved cloud fractions with the model cloud fraction on a global average and according to the satellite sampling: a) maximum cloud overlap assumption and b) random cloud overlap assumption.

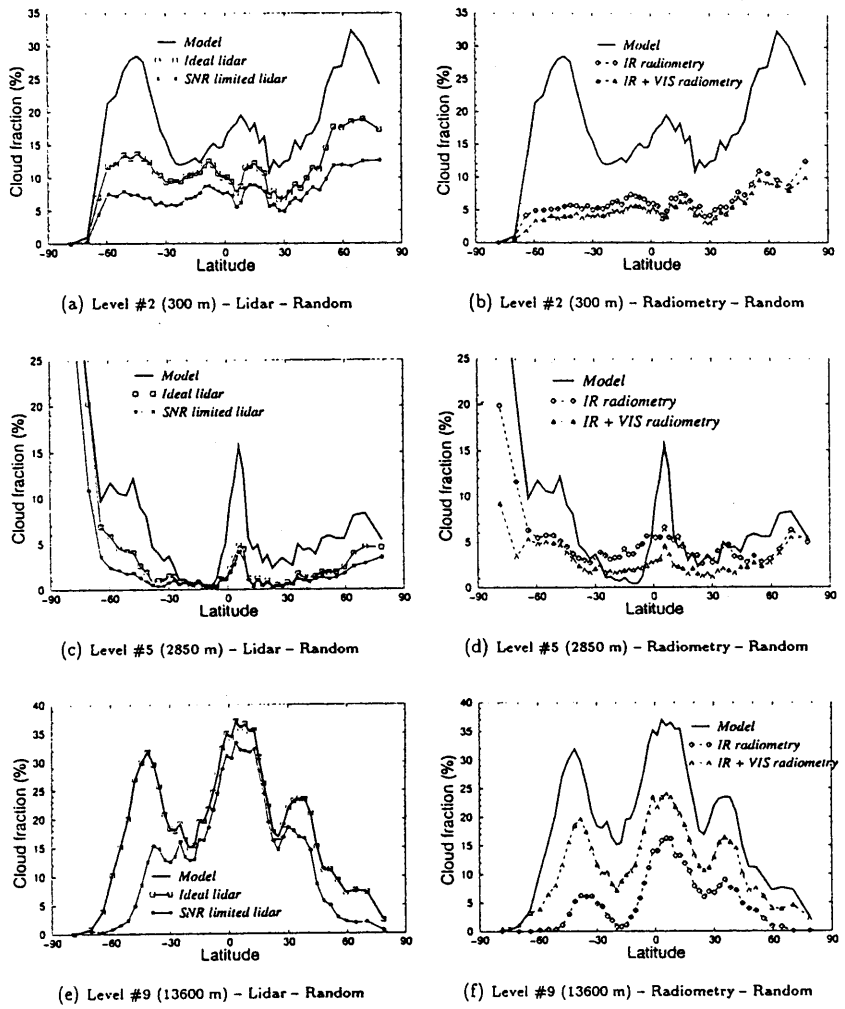

(a) Level #2 (300 m) - Lidar - Random

(b) Level #2 (300 m) - Radiometry - Random

(c) Level #5 (2850 m) - Lidar - Random

(d) Level #5 (2850 m) - Radiometry - Random

(e) Level #9 (13600 m) - Lidar - Random

(f) Level #9 (13600 m) - Radiometry - Random

Figure 7. Zonal mean cloud fraction retrieved by the lidars (left panels) and the radiometers (right panels) for different model levels and for the random cloud overlap assumption.